Ensemble forecast of the Kuroshio meandering

Yasumasa Miyazawa, Shozo Yamane,[1] Xinyu Guo,[2] and Toshio Yamagata[3]

Frontier Research Center for Global Change/Japan Agency for Marine-Earth Science and Technology (JAMSTEC), Kanagawa, Japan

Received 10 April 2004; revised 10 July 2005; accepted 28 July 2005; published 26 October 2005.

[1] Focusing on predictability of the Kuroshio meandering, we have done an ensemble forecast experiment; the application of the method to the problem addressed seems to be the first comprehensive attempt in the community of physical oceanography. By assimilating sea surface height anomaly into an ocean general circulation model in the preceding 40-day period, the observed Kuroshio meandering manifested south of Japan in November 1999 was successfully predicted 2 months before the event. The experiment yields a forecasting skill of the Kuroshio meander position for 60 days in the sense that the RMS error does not exceed the magnitude of the model climatic variation and those obtained from the non-assimilated simulation and persistence. In addition to a single trajectory forecast experiment, ensemble forecasts were conducted using 10 perturbed initial states generated by the breeding method. The predicted states realized as the ensemble members of the 80-day forecast are classified into two categories: large and non-large meander. It is found that the intensity of an anticyclonic eddy in the initial state seems to play a key role in selecting one of the two states.

Citation: Miyazawa, Y., S. Yamane, X. Guo, and T. Yamagata (2005), Ensemble forecast of the Kuroshio meandering, *J. Geophys. Res.*, *110*, C10026, doi:10.1029/2004JC002426.

1. Introduction

[2] The transition of the Kuroshio path between the large-meander state and the non-large-meander one has been extensively investigated by both theoretical and observational studies. The theoretical studies [e.g., *Masuda*, 1982] suggest that the Kuroshio can possess multiple equilibria under the same external conditions. *Kawabe* [1995] discussed the equilibrium states of the Kuroshio system and showed that the large meander appears when the upstream volume transport is relatively large.

[3] As in the atmospheric blocking, we may classify the theoretical studies into two categories: nonlocal [e.g., *White and McCreary*, 1976; *Masuda*, 1982] and local approaches [*Yamagata and Umatani*, 1989]. The former adopts the lee-wave theory for Rossby wave and formulates the Kuroshio bimodality problem as a boundary value problem in which the phase speed C of Rossby wave satisfies suitable inlet and outlet conditions imposed at respective boundaries near the strait south of Kyushu and the one at the Izu-Ogasawara Ridge. In this case, the large-meander state exists when the upstream current U satisfies either subcritical ($U + C < 0$) or critical ($U + C = 0$) conditions. On the other hand, *Yamagata and Umatani* [1987, 1989] demonstrated that for a supercritical condition ($U + C > 0$), the observed large meander can be interpreted as a manifestation of the geometrically trapped nonlinear solitary wave. *Mitsudera and Grimshaw* [1994] extended the theory into a baroclinic case and showed that the specified local topography can generate a stationary large-amplitude wave through baroclinic instability process satisfying a supercritical condition. The observational study of *Kawabe* [1995] supports the local approach at least for the meander formation [*Mitsudera and Grimshaw*, 1994]. Recent modeling studies using realistic topography suggest that even a local seamount south of Japan is important for the formation of the Kuroshio large meander [*Hurlburt et al.*, 1996; *Endoh and Hibiya*, 2001; *Miyazawa et al.*, 2004].

[4] In the framework of the above local approach, transitions between multiple equilibria are governed by initial disturbances if the given state is within the appropriate dynamical regime [*Yamagata and Umatani*, 1987; *Mitsudera and Grimshaw*, 1994]. In fact, this conjecture was tested numerically and the transitions between different states are successfully simulated in some modeling studies [e.g., *Endoh and Hibiya*, 2001]. The Kuroshio volume transport has been either large or intermediate since 1975; however, the stable large meander has not occurred in the last decade (see Quick Bulletin of Ocean Conditions by the Japan Coast Guard) [see also *Qiu and Miao*, 2000]. Therefore, if the real Kuroshio state falls in one of the multiple equilibrium states since 1975, it is interesting to investigate, on the basis of hindcast experiments using a realistic ocean general circulation model (OGCM), how the Kuroshio path variation is sensitive to the initial disturbances.

[5] Recent observational studies using the satellite altimeter and the in situ Acoustic Doppler Current Profilers

[1] Also at Department of Environmental Security, Faculty of Risk and Crisis Management, Chiba Institute of Science, Chiba, Japan.

[2] Also at Center for Marine Environmental Studies, Ehime University, Ehime, Japan.

[3] Also at Department of Earth and Planetary Science, Graduate School of Science, University of Tokyo, Tokyo, Japan.

0148-0227/05/2004JC002426$09.00

(ADCPs) showed that meso-scale eddies are very active south of Japan [*Ebuchi and Hanawa*, 2000]. Regional numerical studies [*Mitsudera et al.*, 2001; *Endoh and Hibiya*, 2001] employing the inflow-outflow boundary conditions also demonstrated that a meso-scale eddy triggers the Kuroshio large meander or offshore non-large meander. *Ebuchi and Hanawa* [2003], using the satellite altimetry data, reported that three offshore non-large meanders in 1993, 1998, and 1999 were triggered by anticyclonic eddies. *Miyazawa et al.* [2004] were successful in simulating the Kuroshio path variation induced by the eddy-Kuroshio interaction using a basin-wide eddy-resolving OGCM.

[6] So far, a few studies have examined possibility of operational numerical predictions of the Kuroshio path south of Japan. *Komori et al.* [2003], using a reduced gravity model initialized by assimilating the TOPEX/Poseidon altimetry data, estimated the predictability limit which falls within the range extending from 30 to 90 days and they further pointed out that the estimate of this kind would heavily depend on the model dynamics employed. *Kamachi et al*. [2004] conducted hindcast experiments of the Kuroshio path during from 1993 to 1999 using an eddy-permitting (1/4° grid) OGCM with the assimilated TOPEX/Poseidon data. The predictability limit of their forecast system is reported to be about 80 days. They suggest that the eddy-Kuroshio interaction is an important potential mediator causing the transition from the nearshore to offshore non-large meander. However, they have not discussed the generation mechanism of the large meander.

[7] In addition to a single trajectory forecast experiment, *Kamachi et al.* [2004] performed an ensemble forecast with five ensemble members accompanying the transition from nearshore to offshore non-large meander. Their ensemble mean forecast yielded slightly better forecasting skill than the unperturbed forecast. However, since their experiment was very preliminary, neither detailed features of the spread in their ensemble experiment nor sensitivity of the prediction on the imposed initial errors was discussed in their study.

[8] No conventional method on ensemble generation has been established yet for multimodal dynamical systems such as the Kuroshio path south of Japan. For a simple dynamical system with multiple attractors, *Miller and Ehret* [2002] evaluated the performance of ensemble runs with several different methods of generation, however, the performance of such a complex dynamical system as the one under consideration remains to be investigated further. As the first step toward such studies, we utilize here an iterative ensemble generation process called ''breeding method'' [*Toth and Kalnay*, 1993]. The breeding method may well simulate the development of growing errors in the assimilation cycle.

[9] In the present study, we discuss the event in the year 1999 using an eddy-resolving OGCM with the TOPEX/Poseidon altimetry data assimilated into the initial field. We conduct a hindcast experiment of the Kuroshio path for a period of 80 days after the last cycle of the assimilated initialization. To the best of our knowledge, the present work is the first comprehensive attempt to investigate the predictability of the Kuroshio meandering using the ensemble forecast approach. Since the eddy dynamics is an important factor in the Kuroshio path variation [*Miyazawa et al.*, 2004], the present use of the eddy-resolving OGCM is vital and enables us to examine meaningful case-by-case variation in the model ensemble.

[10] This paper is organized as follows. In section 2, a hindcast experiment of the event in 1999 as a single trajectory forecast is described. Section 3 covers the results of the ensemble forecast experiment, in particular, the characteristics relating to both the skill and spread in the ensemble run are argued. In section 4, looking into the ensemble forecast of 80 days, we discuss the possible dynamical roles played by eddies in triggering the bifurcation of the bimodal Kuroshio paths. Final section 5 is devoted to summary.

2. Hindcast Experiment of the Kuroshio Meandering

2.1. Ocean Model

[11] The present ocean model is based on Princeton Ocean Model (POM) [*Mellor*, 1998], one of the most popular community models in the world. A high-resolution regional model with spatial grid of 1/12 degree and 35 sigma levels is embedded in a low-resolution basin-wide model with a spatial grid of about 1/4 degree and 21 sigma levels. The inner model domain covers the northwest Pacific (12°N–56°N, 117°E–180°E) and its lateral boundary conditions are determined from the basin-wide model using the one-way nesting method [*Guo et al.*, 2003]. Details of the model configuration are described in our previous paper [*Miyazawa et al.*, 2004].

[12] The model is driven by wind stresses, and heat and salt fluxes. Both wind stress and heat flux fields are calculated from the 6-hourly NCEP/NCAR reanalysis data [*Kalnay et al.*, 1996] using the bulk formula [*Rosati and Miyakoda*, 1988]. Salinity at the ocean surface is restored to monthly mean climatology data [*Levitus et al.*, 1994] with a timescale of 30 days. Simulation of the low-resolution model is started from a state of rest with the annual-mean temperature and salinity fields created from a 1/4 degree climatology data [*Boyer and Levitus*, 1997]. The low-resolution model is spun up by the monthly mean surface forcing for 10 years. Then the model is further driven by 6-hourly surface forcing covering from 1 January 1991 to 30 November 1999. The high-resolution model is also forced from a state of rest with the climatological temperature and salinity fields but with 6-hourly surface forcing applied from 8 August 1996 to 30 November 1999.

2.2. Hindcast of the Kuroshio Meandering in 1999

[13] According to Quick Bulletin of Ocean Conditions published by the Japan Coast Guard (Figure 1, left), the real Kuroshio took an offshore non-large-meander path from November 1999 to June 2001. A hindcast experiment without initialization failed to reproduce this offshore non-large-meander episode. Therefore TOPEX/Poseidon sea surface height anomaly (SSHA) data in the period starting from 26 July to 7 September 1999 have been successively assimilated to the simulated fields in the high-resolution model with the time interval of 10 days.

[14] For indirect estimation of temperature and salinity fields, we adopt a practical approach similar to the optimal analysis equation proposed by *Mellor and Ezer* [1991]. The

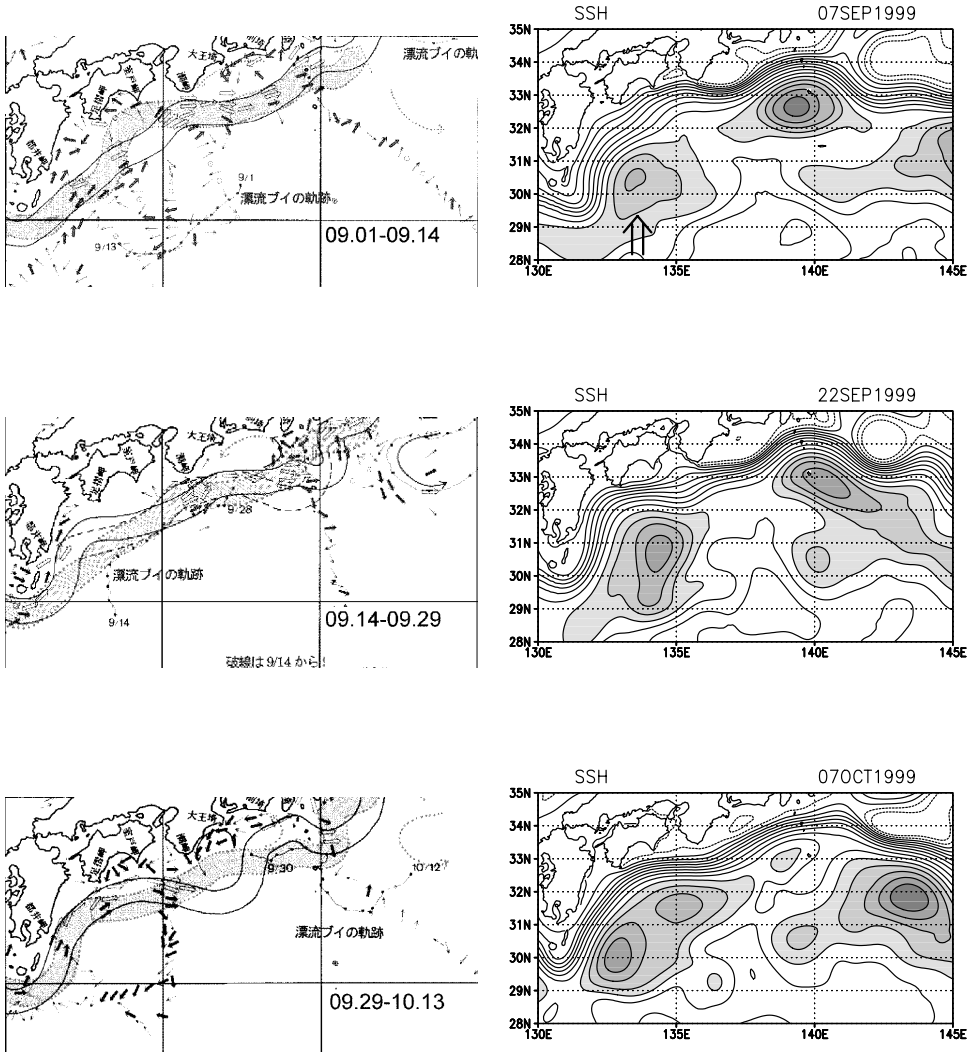

Figure 1. (left) Bi-weakly mean observed Kuroshio path during the period from September 1999 to November 1999, reported in the Quick Bulletin Ocean Conditions provided by Hydrographic and Oceanographic Department, Japan Coast Guard. The gray path corresponds to the last and the white path to the current path. (Right) Model sea surface height in 5-day mean of the unperturbed forecast. Contour interval of sea surface height is 0.1 m.

analyzed estimate of the forecast variable T^f at depths from 50 m to 2000 m is calculated as follows:

$$T^a = T^f + P_{T\eta} F_{T\eta} \left(\Delta\eta^o - \Delta\eta^f \right), \tag{1}$$

where T^a and T^f are analyzed and forecast quantities; $P_{T\eta}$ is a weight of correction and $F_{T\eta}$ is a regression coefficient calculated statistically from the model results without assimilation; $\Delta\eta^o$ and $\Delta\eta^f$ denote the observed and the simulated SSHA, respectively. $\Delta\eta^f$ in equation (1) is calculated by subtracting the temporal mean from the SSH obtained through the one year model simulation in 1998. The observed along-track SSHA referencing to the Ohio University Mean Sea Surface, provided by the Colorado Center for Astrodynamics Research Real-Time Altimeter Data Group [*Lillibridge et al.*, 1997], is interpolated to the model grid with an interval of 10-days using an optimum interpolation method [*Kuragano and Kamachi*, 2000]. The latitudinal mean value of the SSHA corresponding to the large-scale, seasonal variation is subtracted from the SSHA to assimilate only meso-scale variation (Y. Wakata, personal communication, 1999). The weight of correction $P_{T\eta}$ in equation (1) is calculated so that it minimizes the analyzed error $\langle (T^a - T^t)^2 \rangle$, where brackets denote an expected value and T^t represents a true state. $P_{T\eta}$ has the following form:

$$P_{T\eta} = \frac{E_s}{E_o + E_s + 1/C_{T\eta}^2 - 1}, \tag{2}$$

where $E_s = \langle (\Delta\eta^f - \Delta\eta^t)^2 \rangle / \langle \Delta\eta^{t^2} \rangle$ and $E_o = \langle (\Delta\eta^o - \Delta\eta^t)^2 \rangle / \langle \Delta\eta^{t^2} \rangle$ are the normalized simulation and observation error variances of SSHA, respectively. The quantity $C_{T\eta}$ is the correlation coefficient between the SSHA and the temperature/salinity. Derivation of equation (2) is described in Appendix A. The normalized simulation error variance E_s is empirically determined to be 2.8 in the region south of Japan (27°N–38°N, 130°E–145°E) and 1.5 in the other. We conduct ensemble forecasts

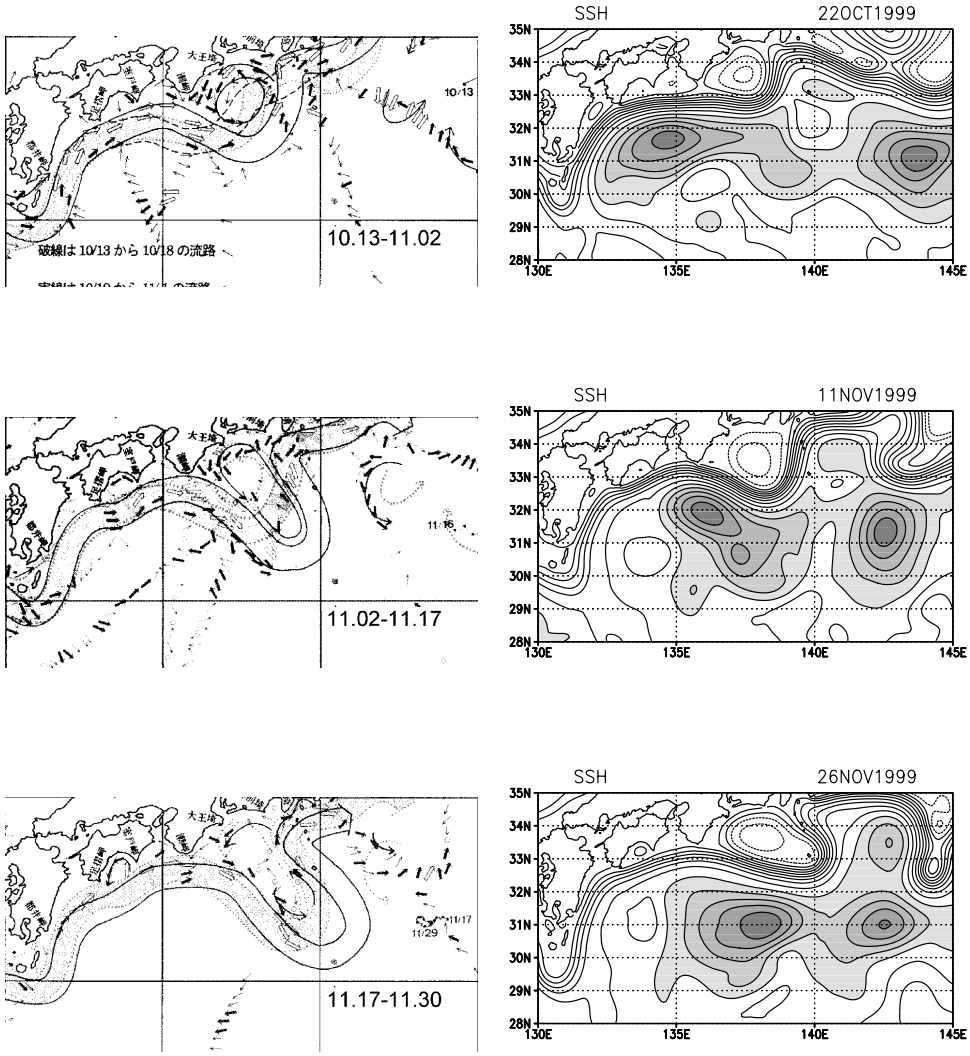

Figure 1. (continued)

to reduce this uncertainty of error estimate. The observation error variance of SSHA may include various types of error (error in the mean SSH used to compute the SSHA, real measurement error of the along-track SSH, interpolation error, etc.), although we simply specify interpolation error variance obtained from the optimum interpolation of along-track SSHA as E_o. The normalizing factor $\langle \Delta\eta^{f^2} \rangle$ as the variance of true SSHA is to be substituted by the variance of observed SSHA, since there is no other way to give an approximate estimate of this quantity.

[15] In order to achieve smooth assimilation, both temperature and salinity fields are nudged to the analyzed variables in equation (1) with a restoring timescale of 0.3 days during a tentatively set time span of 6 days in the middle of which observational data are provided. The nudging toward both the analyzed temperature and salinity gradually would modify velocities and sea surface height through geostrophic adjustment. The analysis (1) is calculated using the temperature/salinity and SSHA fields forecasted at 3 days before the observation time. The grid data of SSHA created from 26 July 1999 to 7 September 1999 were assimilated into the original simulation. Then the time integration proceeded with constant surface forcing and lateral boundary condition evaluated at the last initialization time.

[16] Figure 1 (right) shows evolution of the assimilated sea surface height after the last initialization. The anticyclonic eddy stays southeast of the Kyushu Island in the initial state. Then it propagates eastward toward the Kii Peninsula in October 1999 and generates the meander in November 1999 as observed (left panel of Figure 1, left). Thus we see that the initialization with the aforementioned data assimilation processes leads to a successful prediction of the meander of the Kuroshio, though the predicted field on 26 November 1999 underestimates the meander amplitude with its position shifted to the east compared with the observation.

[17] To measure the forecasting skill quantitatively, we use both RMS error $e_1 = \sqrt{\overline{(\eta^f - \eta^r)^2}}$ and anomaly correlation of sea surface height $c_1 = \dfrac{\overline{\Delta\eta^f \Delta\eta^r}}{\sqrt{\overline{\Delta\eta^{f^2}} \cdot \overline{\Delta\eta^{r^2}}}}$ for a reference sea surface height η^r, where $\overline{A} \equiv \dfrac{1}{N}\sum_{j=1}^{N} A_j$ (N denotes number of grid points in the Kuroshio region; 28°N–35°N, 130°E–140°E); the RMS error is normalized by the value 0.19 m

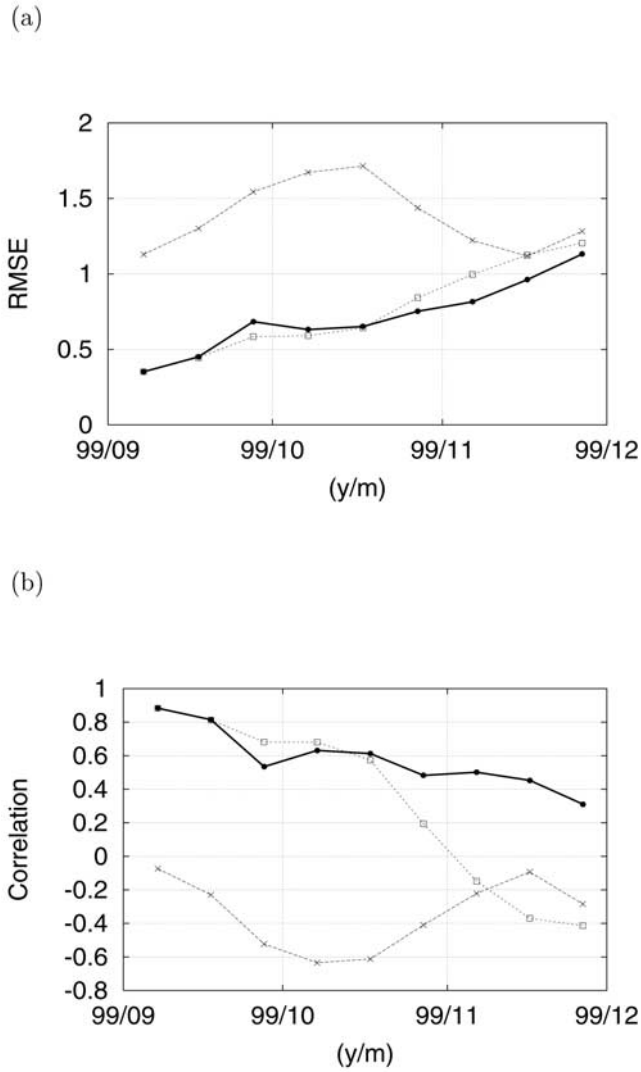

Figure 2. (a) Evolution of RMS errors of sea surface height anomaly for the reference run over the Kuroshio region, 28°N–35°N, 130°E–140°E. The RMS error is normalized by RMS variability of the simulation in the same region (0.19 m). Thick line with solid circles corresponds to the unperturbed forecast. Long dashed line with crosses corresponds to the non-assimilated simulation run. Short dashed line with squares corresponds to the persistence of an initial state. (b) As in Figure 2a except for anomaly correlation.

which is the RMS variation in the Kuroshio region calculated from the one year model simulation in 1998. In the reference assimilation run, we utilize not only the TOPEX/Poseidon but also the ERS-2 data to effectively approximate a true state. We call this additional assimilation run simply as the reference run. Figure 2a exhibits that a skill of the forecast (thick line with solid circles) is superior to those of non-assimilated simulation (long dashed line with crosses) and persistence (short dashed line with squares) during the meander period from 27 October to 26 November. Another measure of skill, anomaly correlation, also shows some similar feature as the RMS error (Figure 2b). The skill improvement of the forecast, however, measured by the RMS error seems to be smaller than that by the anomaly correlation. Although the pattern of the forecast SSHA is generally similar to the reference SSHA even in the late period, stronger signal of the reference SSHA than that of the forecast, especially in the meandering region (not shown), tends to increase the RMS error. The RMS error exceeds the level of the modeled climatic variation more than 70 days after the last initialization, while the persistence reaches the level at 60 days. Therefore the forecast only improves on the persistence by 10 days. Skills of both the unperturbed and ensemble mean forecasts for SSHA and other variables (temperature, salinity, and the Kuroshio meander position) are further discussed in the next section.

3. Ensemble Forecast

[18] Ensemble forecasts were conducted using 10 perturbed initial states generated by the breeding method [*Toth and Kalnay*, 1993]. First, on 26 July 1999, two-dimensional random perturbation $\Delta\eta_{ptb}$ with a horizontal correlation scale of 0.7 degree [*Evensen*, 1994] is added to the analyzed value T_c^a of the assimilation run described in section 2, in the region (27°N–38°N, 130°E–145°E) with upper 1000 m depth,

$$T_{ptb}^a = T_c^a + F_{\eta T}\Delta\eta_{ptb}, \tag{3}$$

where $\Delta\eta_{ptb}$ is assumed to have zero mean and RMS magnitude of 0.05 m. At every assimilation time during the

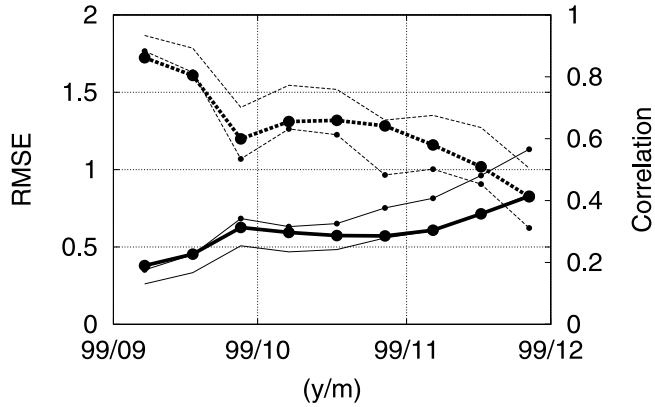

Figure 3. Evolution of RMS errors of sea surface height anomaly normalized by RMS variability of the simulation (0.19 m) for the reference run over the Kuroshio region, 28°N–35°N, 130°E–140°E (solid lines with solid circles) and anomaly correlations (dashed lines with solid circles). Thick lines with solid circles denote the ensemble mean and thin lines with solid circles denote the unperturbed forecast. Thin solid and dashed lines denote theoretical skill, $\langle e_M^2\rangle^{1/2} = \sqrt{(M+1)/2M}\langle e_1^2\rangle^{1/2}$ and $\langle c_M\rangle = \left\{\frac{M}{1+(M-1)\langle c_1\rangle}\right\}^{1/2}\langle c_1\rangle$ estimated from the unperturbed forecast values, respectively (M = 10).

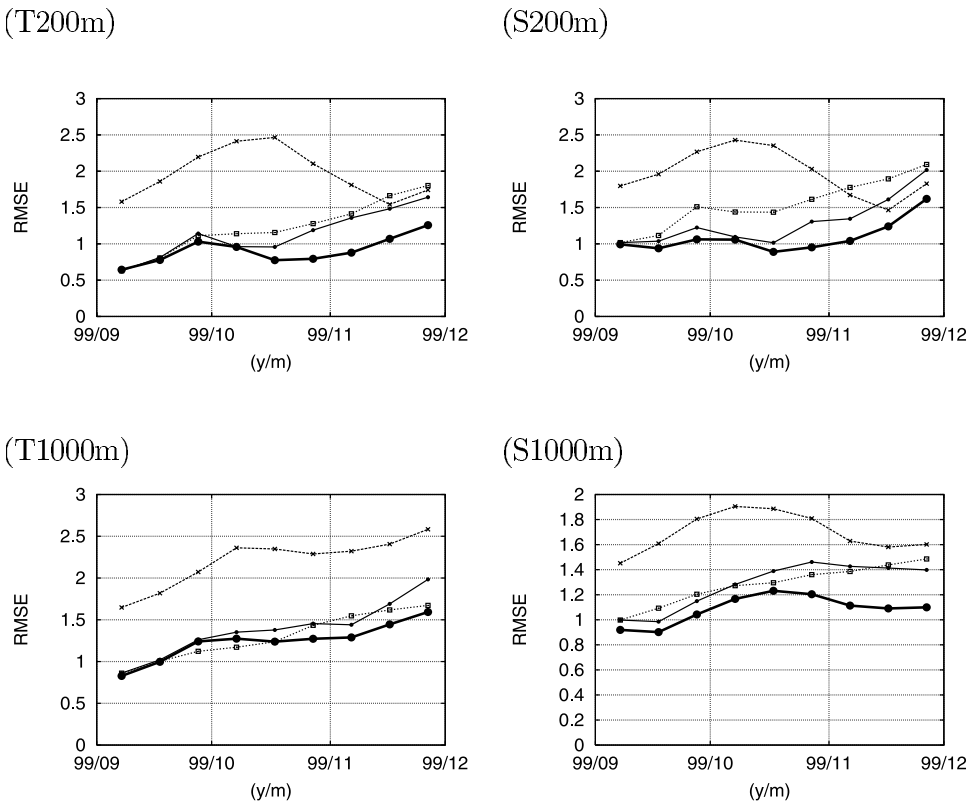

Figure 4. Evolution of RMS errors of (left) temperature and (right) salinity normalized by RMS variability of the simulation for the reference run over the Kuroshio region, 28°N–35°N, 130°E–140°E. The RMS variability values of temperature at 200 m and 1000 m are 1.1 and 0.28°C, respectively. Those of salinity are 0.043 and 0.020 psu, respectively. Thick lines with solid circles denote the ensemble mean and thin lines with solid circles denote the unperturbed forecast. Long dashed line with crosses denotes the non-assimilated simulation run. Short dashed line with squares denotes the persistence of an initial state.

period from 5 August to 7 September 1999, the difference of sea surface height anomaly (SSHA) between the perturbed run $\Delta\eta^f_{ptb}$ and the assimilation run $\Delta\eta_c$ is added to the assimilated value as follows:

$$T^a_{ptb} = T^a_c + F_{\eta T} C_{0.05m}\left(\Delta\eta^f_{ptb} - \Delta\eta_c\right), \tag{4}$$

where $C_{0.05m}$ is a coefficient to make RMS value of $C_{0.05m}(\Delta\eta^f_{ptb} - \Delta\eta_c)$ equal to 0.05 m. For the sake of simplicity, we rescale only SSHA. 10 ensemble members are created by repeating the breeding method staring from 10 random perturbations $\Delta\eta_{ptb}$ uncorrelated with each other.

[19] Simple analytical relationships between the forecast skill and properties of our ensemble forecast may be derived under following assumptions: (1) the model is perfect and forecast error growth is caused only by initial state error through internal dynamics of the model, (2) each individual integration in an ensemble is equally likely to represent the true state evolution, and (3) an initial ensemble represents true analysis error distribution within sampling limits [*Murphy*, 1988]. The ensemble mean forecast is expected to have better forecasting skill statistically than an unperturbed forecast by smoothing out small-scale features, which are significantly influenced by the uncertainty of the initial state. Theoretical estimate of RMS error of ensemble mean forecast for M ensemble members is

$$\langle e^2_M \rangle^{1/2} = \sqrt{(M+1)/2M}\,\langle e^2_1 \rangle^{1/2}, \tag{5}$$

where e_M and e_1 are RMS errors of an ensemble mean forecast and a single forecast, respectively; brackets denote an expected value [e.g., *Murphy*, 1988]. An additional assumption that variations in anomaly intensity are small yields an estimate of anomaly correlation of the form

$$\langle c_M \rangle = \left\{\frac{M}{1+(M-1)\langle c_1\rangle}\right\}^{1/2}\langle c_1\rangle, \tag{6}$$

where c_M and c_1 are anomaly correlations of an ensemble mean forecast and a single forecast, respectively [*Murphy*, 1988]. These two theoretical relations indicate that ensemble mean forecast is better in the skill than a single forecast on average. We investigate the skill measured by both the RMS error and anomaly correlation averaged over the Kuroshio region (28°N–35°N, 130°E–140°E) in an ensemble forecast experiment, where the theoretical relations are not necessarily satisfied.

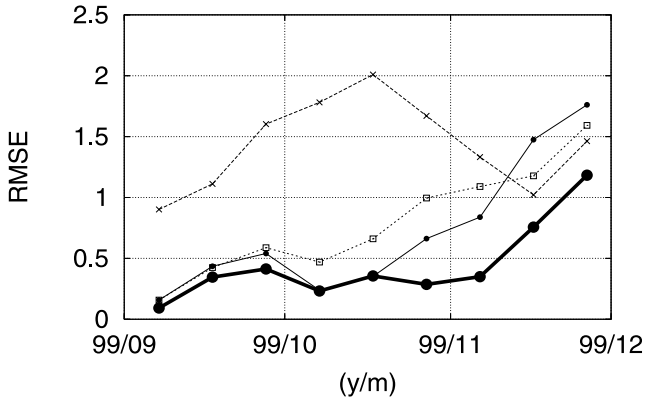

Figure 5. As in Figure 4 except for RMS error of the Kuroshio axis (0.4 m contour of sea surface height) along the meandering region, 135°E–140°E. The RMS variability of the Kuroshio axis is 49.6 km.

[20] Figure 3 compares forecasting skills of sea surface height anomaly (SSHA) in ensemble mean measured by both the RMS error (solid line with solid circles) and anomaly correlation (dashed line with solid circles) with those of the unperturbed forecast. The RMS error of the ensemble mean forecast is comparable with that of the unperturbed forecast during the early period from September to October. The disagreement of ensemble mean skill with a theoretical estimate (thin solid line) during the early period is due to non-satisfaction of the second assumption mentioned above; that is, the unperturbed forecast represents the true state evolution better than the each perturbed forecast during the early period. During the late one from the end of October to a month later, however, the skill of the ensemble mean forecast shows some improvement; the RMS error almost agrees with the theoretical estimate (thin solid line). This implies that the skill of the unperturbed forecast is no longer better than that of each perturbed forecast during the late period. Anomaly correlation also indicates the improvement of the skill in the ensemble mean forecast during the late period, though the improvement is not so evident as that of the RMS error.

[21] We also evaluate the forecasting skill for temperature and salinity (Figure 4). Both temperature and salinity may be less predictable than SSHA because, in almost all cases, the RMS error exceeds the magnitude of the climatic variation soon after or in the beginning of the forecast. Introduction of another data (ERS-2) into the data assimilation for the reference run may have more impact on temperature and salinity than on SSHA. Near the surface, as shown in upper panels of Figure 4, the forecast shows better skill than both the persistence and non-assimilated simulation, and the ensemble mean forecast improves the skill of the unperturbed forecast. These features are consistent with those discussed in the forecast of SSHA, which is strongly affected by density in the surface layer. In the depth of 1000 m, the unperturbed and ensemble mean forecasting skills are comparable to the persistence (Figure 4, bottom). Below 1000 m, both temperature and salinity vary slightly in time of duration (not shown).

[22] A skill measure of most interest is position of the Kuroshio meander. We define sea surface height (SSH) contour of 0.4 m as the axis of the Kuroshio south of Japan (e.g., see Figure 8 later in this section). 0.4 m contour of SSH well agrees with 15°C contour at depth of 200 m (not shown), which is traditionally used to capture the Kuroshio path [e.g., *Kawai*, 1969]. As shown in Figure 5, the forecasting skill of the meander position is clearly better than that of the persistence. The skill improvement by the ensemble mean is also evident. While the error of the unperturbed forecast exceeds those of both the persistence and non-assimilated simulation after 70 days, the ensemble mean has some skill at this time.

[23] The spread of the ensemble provides useful information about predictability; the growth of spread indicates loss of forecasting skill. Here we adopt the RMS difference of individual ensemble members from the ensemble mean as a measure of the ensemble spread. Figure 6 indicates that the spread gradually increases with reduction of the forecast skill shown in Figure 2. Theoretical relation between spread and RMS error of a single forecast is given by $\langle s_M^2 \rangle = \frac{M-1}{2M}\langle e_1^2 \rangle$ under the theoretical assumptions. Since the relation of RMS error is given by $\langle e_M^2 \rangle = \frac{M+1}{2M}\langle e_1^2 \rangle$, we have the relation: $\frac{\langle s_M^2 \rangle (M+1)}{\langle e_M^2 \rangle (M-1)} = 1$ [e.g., *Takano*, 2002]. Figure 7 shows the time sequences of $\frac{\langle s_M^2 \rangle (M+1)}{\langle e_M^2 \rangle (M-1)}$ calculated from RMS errors and difference respectively given in Figures 3 and 6. Roughly speaking, the value of the quantity averaged through the whole period is nearly one. This quantity, however, shows temporal variations; the value less than one in the early period becomes larger in October and exceeds one early in November. Its increasing tendency may be connected with a relatively rapid increase of the ensemble spread late in October shown in Figure 6. The rapid increase of the spread seems to be related to the bifurcation of the Kuroshio path, as is discussed in the next paragraph.

[24] Figure 8 shows "spaghetti" diagram of the Kuroshio path on 26 November 1999. The predicted Kuroshio me-

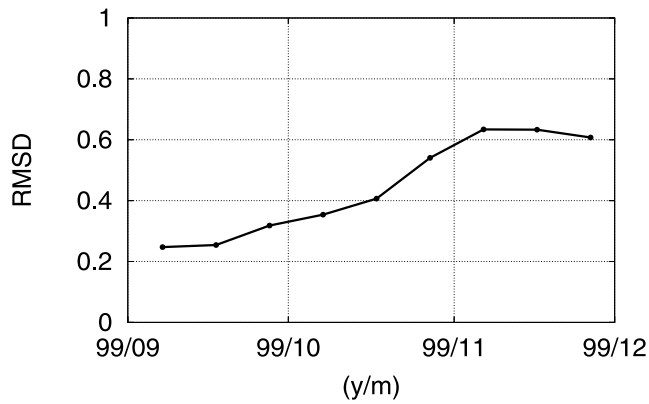

Figure 6. Evolution of ensemble spread, S_M, measured by RMS difference normalized by RMS variability of the simulation (0.19 m) for the reference run over the Kuroshio region, 28°N–35°N, 130°E–140°E.

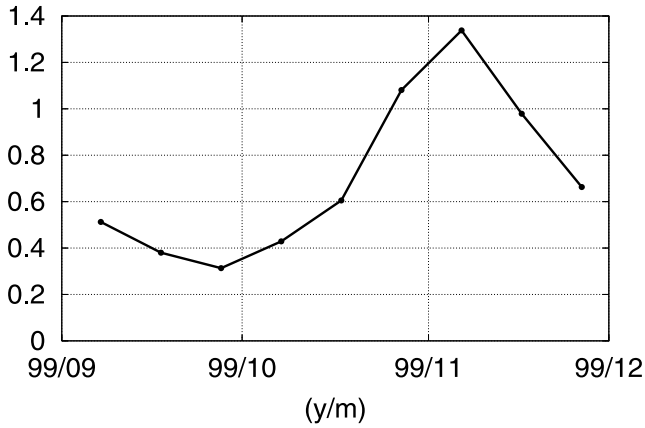

Figure 7. Evolution of $\frac{\langle s_M^2 \rangle (M+1)}{\langle e_M^2 \rangle (M-1)}$ (M = 10) in the Kuroshio region, 28°N–35°N, 130°E–140°E.

ander defined as the ensemble mean of the 80-day forecast (thick curve) has larger amplitude in the region west of 140°E than the unperturbed forecast (dashed curve), which might be consistent with both Quick Bulletin of Ocean Conditions (lowest left panel of Figure 1) and the reference run (dash-dotted curve). However, since the Kuroshio path variation south of Japan has the multimodal structure [e.g., *Kawabe*, 1995], we must be careful in interpreting the ensemble mean forecast. Figure 8 indicates that the 80-day forecast ensemble members (thin curves) of the Kuroshio path south of Japan are classified into three patterns: weak meander (two members), weak meander east of the Izu Islands (three members), and strong meander (five members). The ensemble mean forecast of the present case seems to be a mixture of the multimodal states. Exact skill evaluation of the ensemble mean forecast of the Kuroshio path variation needs more experiments for more various situations. In the present study, attention is focused on the variation of the Kuroshio path generated by the ensemble forecast.

[25] The resulting Kuroshio paths shown in Figure 8 are characterized by indices calculated from sea surface variables. Figure 9a shows the time evolution of the sea level at 32.5°N, 138°E for each ensemble forecast. The index exhibits clear difference in the Kuroshio meander amplitude; low (high) level indices correspond to strong (weak) meander. The unperturbed forecast reproduces a weak meander east of the Izu Islands.

[26] It is well known that the change of the Kuroshio path is associated with sea level changes along the southern coast of Japan [*Kawabe*, 1995]. According to the tide gauge data, the deviation from long-time mean of the sea level difference between Kushimoto and Uragami (see Figure 8 for locations) during the large-meander state is negative (about −10 mm) and less susceptible to change. As shown in Figure 9b, although all ensemble members predict reduction of the sea level difference between Kushimoto and Uragami, three members corresponding to the weak meander east of the Izu Islands show some rise in the sea level difference in November. The sea level at Hachijojima (see Figure 8 for location) is used as another path index of the Kuroshio axis which characterizes two non-large-meander states: the offshore non-large meander (low level) and the nearshore non-large meander (high level). The typical large-meander state is also characterized by high sea level at Hachijojima. The sea levels at Hachijojima in the ensemble members bifurcate into low and high states in November 1999 (Figure 8c); the low sea level appears in the three members corresponding to the weak meander east of the Izu Islands. In short, the Kuroshio path indices obtained from the members of the strong meander found in Figure 8a have more similar features to the large meander than those obtained from the members of weak meander, which correspond to the nearshore or offshore non-large meander. In the next section, we will discuss the predictability of the Kuroshio meandering south of Japan from the viewpoint of eddy dynamics triggering and leading to the remarkable difference found in the 80 days ensemble forecast.

4. Predictability of the Kuroshio Meandering

[27] We plot the relation between the intensity of the initial trigger eddy and resulting meander amplitude of the ensemble forecasts in Figure 10. Although the 50 days ensemble forecasts do not bifurcate into two branches yet (Figure 10a), striking path bimodality manifests itself in the 80 days ensemble forecasts. Therefore the path state within the 50 days is more predictable. Figure 10b indicates that strong anticyclonic eddies may basically induce the large meander. We note that one member stays at a weak meander state. In the latter case, the initial anticyclone is distorted and eventually splits into two weak anticyclones in September 1999. Then the weak anticyclone causes the weak meandering in November 1999. Note that the bifurcation of the meander types has no dependence on the upstream volume transport of two kinds: the Kuroshio mainstream in the East China Sea and the Ryukyu current east of the Nansei Islands. For ensemble members, the volume transport of the Kuroshio mainstream measured across the PN-line in the East China Sea ranges from 29 to 33 Sv.

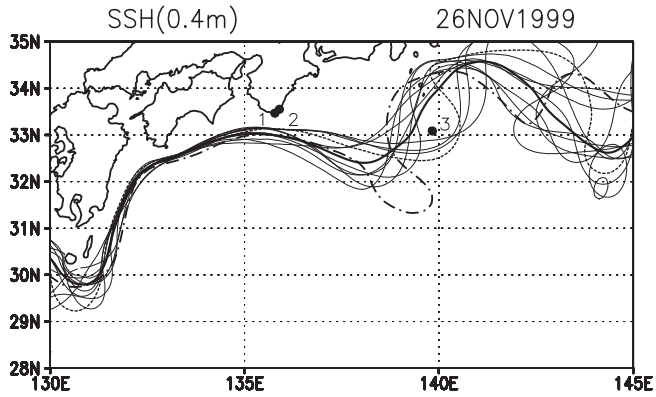

Figure 8. "Spaghetti" diagram of the Kuroshio path on 26 November 1999. The Kuroshio path is defined as a curve on which the value of sea surface height equals 0.4 m. Thick curve denotes ensemble mean. Thin curves correspond to individual ensemble members. Dashed curve denotes the unperturbed forecast. Dash-dotted line denotes the reference run. The numbers denote the tide stations: 1, Kushimoto; 2, Uragami; 3, Hachijojima.

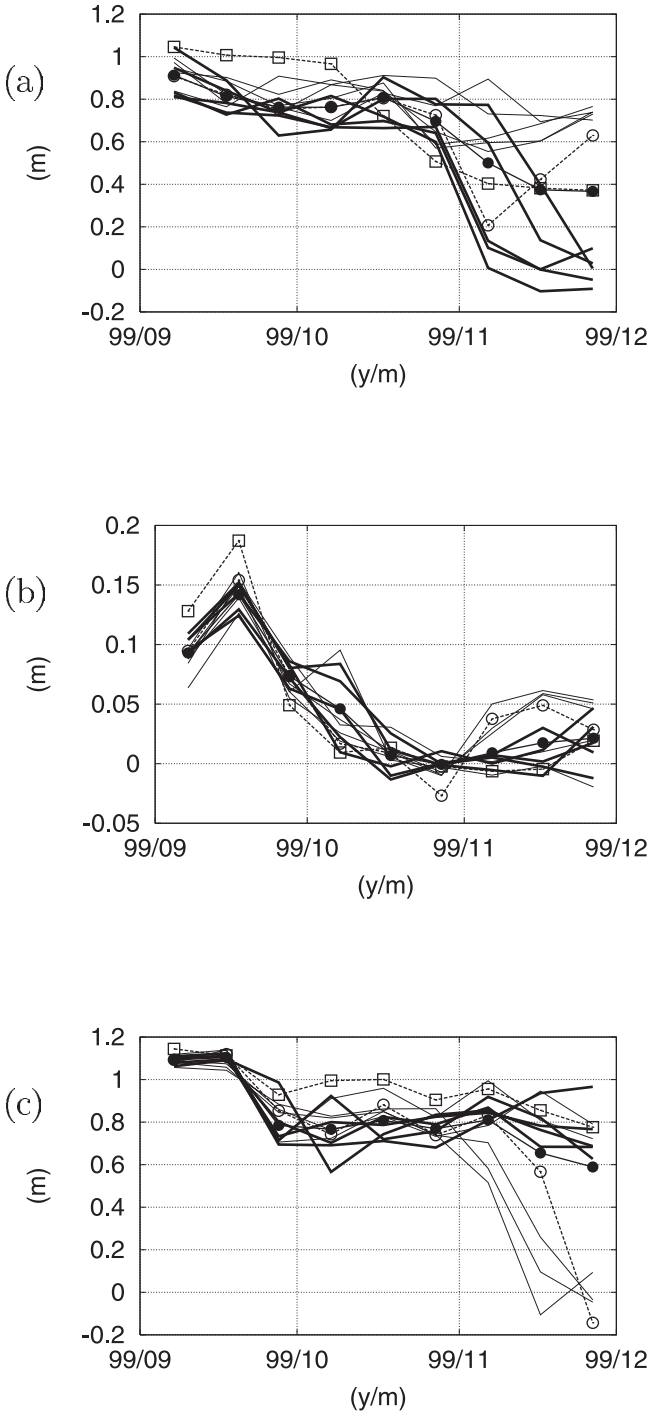

Figure 9. (a) Evolution of sea level at 32.5°N, 138°E. Thick and thin solid lines correspond to ensemble members of strong and weak meander, respectively. Solid line with closed circles denote ensemble mean. Dashed line with open circles denotes the unperturbed forecast. Dashed line with open squares denotes the reference run. (b) As in Figure 9a except for sea level difference between Kushimoto and Uragami. (c) As in Figure 9a except for sea level of Hachijojima.

[28] The previous studies [*Hurlburt et al.*, 1996; *Endoh and Hibiya*, 2001; *Miyazawa et al.*, 2004] have suggested that baroclinic energy conversion is related to the deep anticyclonic circulation associated with the Kuroshio meander. Figure 11 shows time evolution of the kinetic energy at the depth of 4000 m averaged in the area of 31°N–33°N, 135°E–138°E. The large kinetic energy associated with the deep anticyclonic circulation is certainly found in ensemble members producing the large meander (solid curves) in the 80-day forecast on 26 November 1999. However, the deep anticyclonic circulation is not yet excited in the 50-day forecasts on 27 October 1999. This difference is consistent with the characteristics of the meander growth shown in

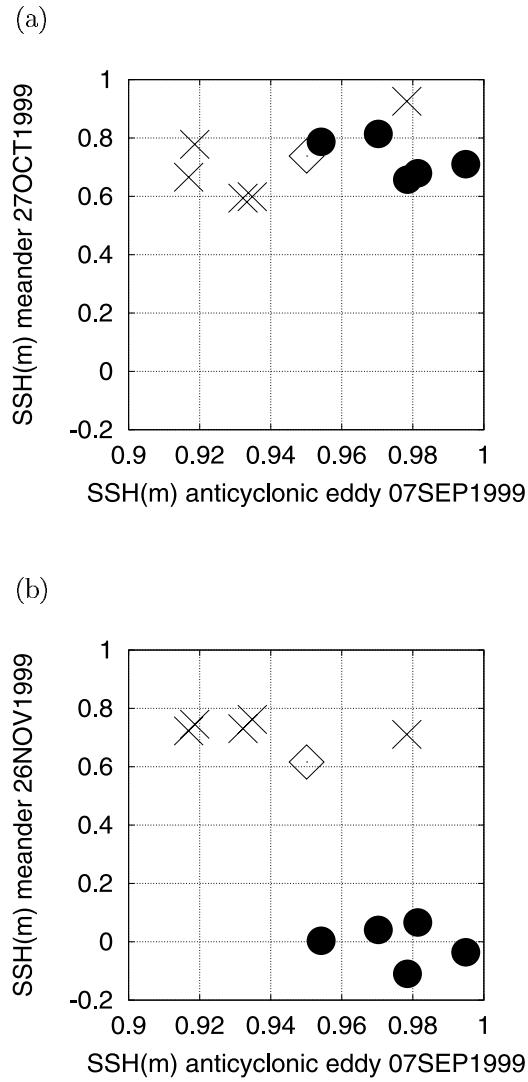

Figure 10. (a) Relations between intensity of the trigger anticyclonic eddy (mean over a region in which sea surface height exceeds 0.9 m within the Kuroshio region, 28°N–32°N, 130°E–136°E) and the Kuroshio meander amplitude (sea surface height at 32.5°N, 138°E) on 27 October 1999. Solid circles correspond to ensemble members of the large meander. Crosses correspond to ensemble members of the non-large meander. A diamond corresponds to the unperturbed forecast. (b) As in Figure 8a on 26 November 1999.

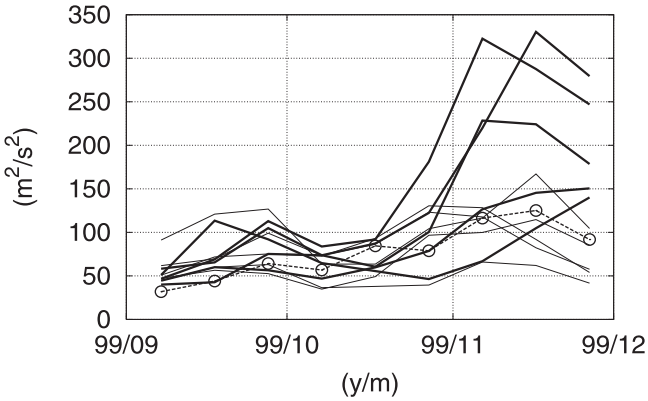

Figure 11. Evolution of kinetic energy (in $m^2\ s^{-2}$) at the depth of 4000 m averaged over 31°N–33°N, 135°E–138°E. Thick solid lines correspond to ensemble members of the large meander. Thin solid lines correspond to individual ensemble members of the non-large meander. Dashed line with open circles denotes the unperturbed forecast.

Figure 10. We note that no difference is found in the kinetic energy of initial ensemble members.

[29] Figure 12 compares evolution of the anticyclonic eddy activities depicted at sea surface height (upper 0.9 m) and deep flow field in three different paths: the nearshore non-large meander (nNLM), offshore non-large meander (oNLM), and large meander (LM). We can recognize clear intensity difference of the anticyclonic eddy southeast of Kyushu in the initial states. As the Kuroshio meander grows in November, both the upper and lower layer anticyclones in the LM case are significantly intensified compared with the NLM cases. We calculate the barotropic eddy kinetic energy (Figure 13a), $\frac{1}{2}(u'^2 + v'^2)$, where u', v' are deviations of horizontal velocities from time mean, and available potential energy (Figure 13b), $\frac{g^2}{2N_b^2}\left(\frac{\rho'}{\rho_0}\right)^2$, where g is gravity acceleration; N_b is background buoyancy frequency; ρ' is deviation of density from time mean; ρ_0 is constant reference density, averaged within the anticyclonic eddy. The eddy kinetic energy of the trigger eddy in ensemble members producing the large meander is generally larger than that in other ensemble members. The available potential energy in the members of the large meander generally increases after early October, when the anticyclone collides with the Kuroshio. Figure 13 suggests that the energy of the trigger eddy is affected by the interaction between the Kuroshio and the anticyclone, which may be intensified by stronger anticyclone in the initial state. To guess the energy source associated with the eddy-Kuroshio interaction, we also calculate both the eddy kinetic energy and available potential energy averaged in the Shikoku basin as shown in Figure 14. After early October, the eddy kinetic energy increases and the available potential energy decreases generally in all members. These features seem to be interestingly emphasized in the ensemble members of the large meander. However, it is beyond the scope of the present study to analyze energy flows in detail related to the complicated eddy-Kuroshio interaction.

[30] To specify a timescale of the trigger eddy, we introduce three non-dimensional parameters governing the geostrophic dynamics on a beta plane: the beta parameter ($\hat{\beta} = \beta L/f$), stratification parameter ($\hat{s} = (R_d/L)^2$), and Rossby number ($\hat{\varepsilon} = \hat{s}\Delta H_1/H_1$) [*Pedlosky*, 1987]. The notations employed here are as follows: f is the Coriolis parameter ($7.3 \times 10^{-5}\ s^{-1}$), β the meridional gradient of f ($2.0 \times 10^{-11}\ s^{-1}\ m^{-1}$), L the horizontal length scale (120 km), R_d the internal deformation radius (40 km at 30°N according to *Emery et al.* [1984]), H_1 depth of the thermocline (550 m), and ΔH_1 is variation of the thermocline (50 m to 80 m for depth of 26.5 sigma-t). For the anticyclonic eddies in the ensemble initial states, we have $\hat{\beta} = 0.033$, $\hat{s} = 0.11$, and $\hat{\varepsilon} = 0.010 - 0.016$. This suggests that they fall into the subset of the planetary geostrophic regime (PG2) of *Williams and Yamagata* [1984] or the frontal geostrophic regime of *Cushman-Roisin* [1986]). If we introduce a two-layer model, the inverse timescale of the frontal geostrophic eddy is given by $\omega = (H_1/H)\hat{\varepsilon} = (P_2/P_1)\hat{\varepsilon}$ [*Cushman-Roisin et al.*, 1992], where H is the total depth of 4000 m; P_1, P_2 are pressure scales of the upper and lower layers, respectively. For the eddies in the ensemble experiments, this timescale ranges from 72 days to 115 days. It is determined by the slow lower-layer velocity field related to pressure P_2 there. The timescale might be consistent with the limit of the predictability in the present study, i.e., 50–80 days. The OGCM simulation suggests that the timescale of the trigger eddy is longer than timescale due to advection by the Kuroshio mainstream, i.e., 10 days. The timescale of the predictability is related to behavior of the eddy itself rather than simple advection of the eddy by the Kuroshio.

5. Summary

[31] We have demonstrated that our forecast with a state-of-the-art OGCM initialized on 7 September 1999 by assimilating sea surface height data successfully predicts the meandering of the Kuroshio south of Japan as observed in November 1999. The experiment yields a forecasting skill of the Kuroshio meander position for 60 days in the sense that the RMS error does not exceed the magnitude of the model climatic variation and those obtained from the non-assimilated simulation and persistence (Figure 5). The timescale agrees with that evaluated by the previous studies [*Komori et al.*, 2003; *Kamachi et al.*, 2004].

[32] While we obtained the hopeful results from the ensemble forecast experiment, further extensive studies of this kind are needed to assess the effects of the ensemble forecast on the forecast skill. In the present study, we focused our attention on the transitions from the nearshore

Figure 12. Snapshots of sea surface height upper 0.9 m (contour interval is 0.1 m) and horizontal velocity at 4000 m depth. (left) An ensemble member corresponding to the nearshore non-large meander. (middle) The unperturbed forecast, which realizes the offshore non-large meander. (right) An ensemble member corresponding to the large meander.

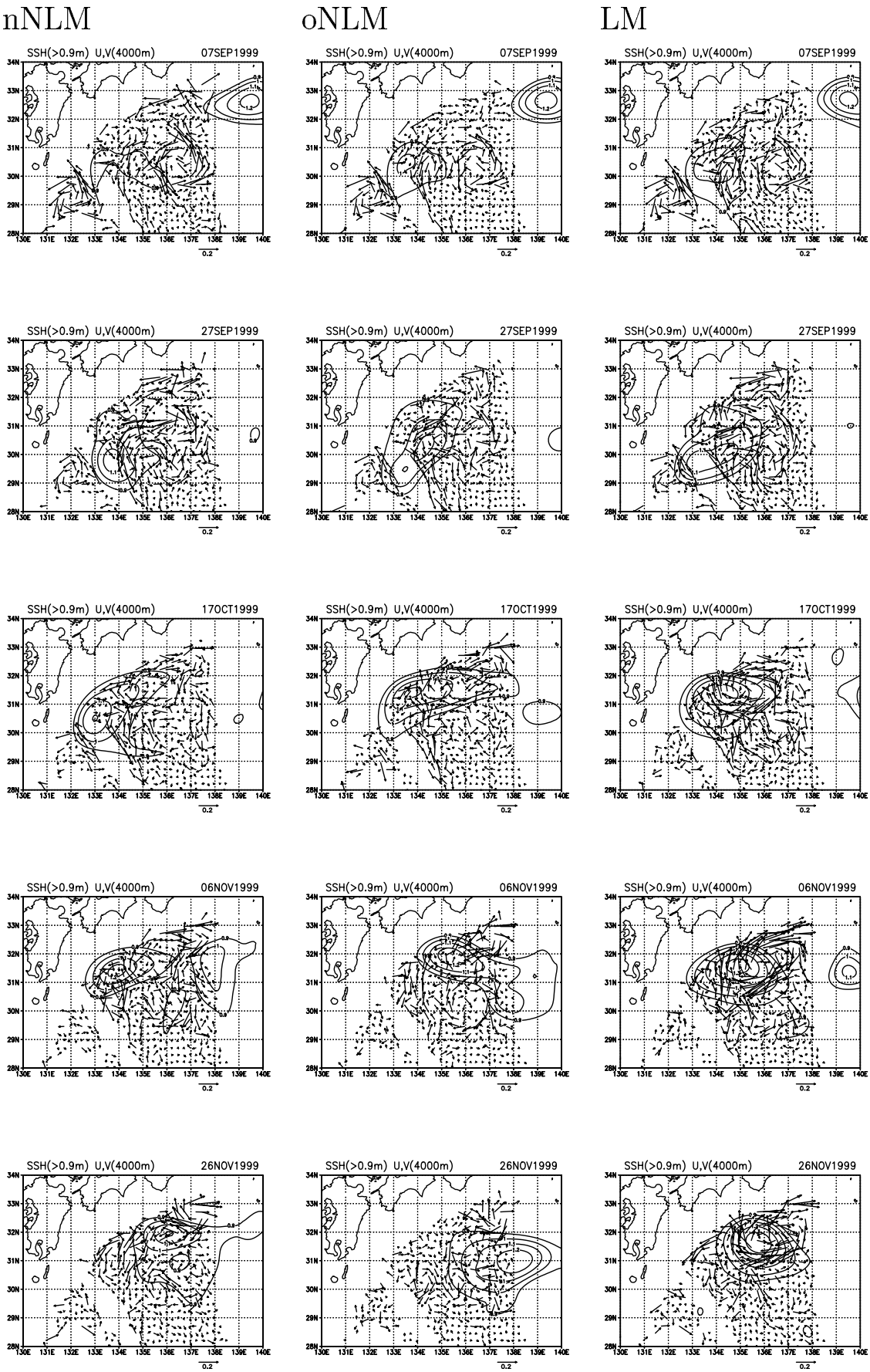
nNLM
oNLM
LM
SSH(>0.9m) U,V(4000m) 07SEP1999
SSH(>0.9m) U,V(4000m) 27SEP1999
SSH(>0.9m) U,V(4000m) 17OCT1999
SSH(>0.9m) U,V(4000m) 06NOV1999
SSH(>0.9m) U,V(4000m) 26NOV1999

Figure 12

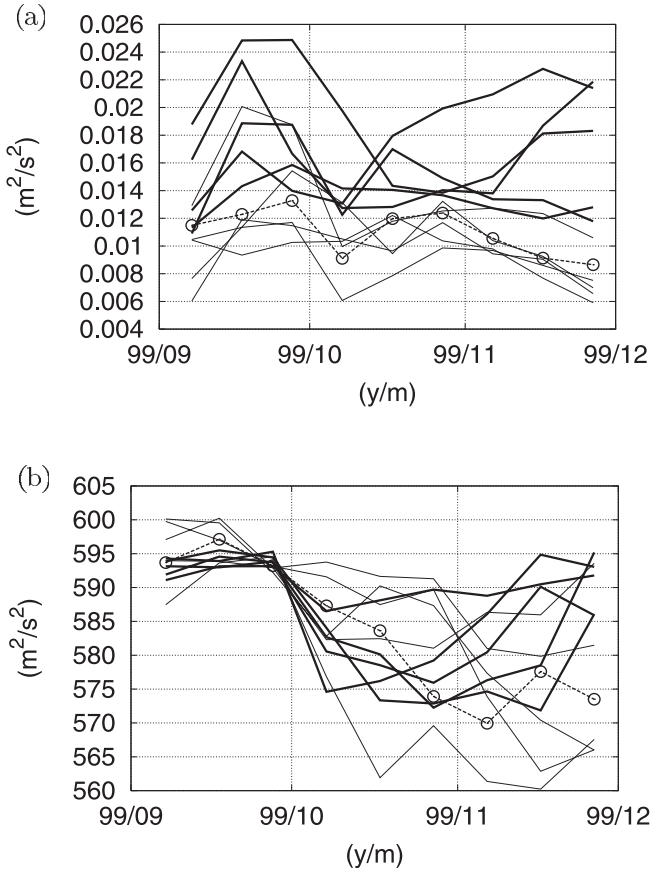

Figure 13. (a) As in Figure 11 except for eddy kinetic energy (in m^2 s^{-2}) of the trigger anticyclonic eddies (a region in which sea surface height exceeds 0.9 m, averaged over 28°N–32°N, 130°E–136°E in September 1999 and over 29°N–32.5°N, 133°E–140°E in October and November 1999). (b) As in Figure 13a except for available potential energy (in m^2 s^{-2}) of the trigger anticyclonic eddy.

non-large meander to the large or offshore non-large meander. The meanders occurred in the ensemble members for the 80-day forecast are classified into two categories: the large meander and the non-large meander. The bifurcation occurs more than 50 days after the initialization. In the present case, the ensemble mean of the 80-day forecast seems to be a mixture of the multimodal states, which might be similar to climatological mean state of the Kuroshio path. The theoretical relations (5) and (6) hold when the ensemble spread agrees with the natural variation owing to loss of predictability; the ensemble mean corresponds to the climatological mean. Moreover, in the multimodal system such as the Kuroshio path south of Japan, the ensemble mean may not be a physically-realizable state. We also notice that the present use of the reference assimilation run as the "truth" may lead to either an over- or under-estimation of the forecast skill since the theoretical relations (5) and (6) of the ensemble forecast pertain to the "real" error variance. Skill improvement using the ensemble mean forecast would be validated by conducting many forecast experiments for various situations of the Kuroshio path transition.

[33] A novel feature we found in our experiments presented here is a fact that the intensity of an initial anticyclonic eddy plays a key role for the subsequent development of the Kuroshio meander classified into two categories, i.e., a strong anticyclone induces the large meander. Figure 10 suggests that a critical level of the intensity exists. 0.05 m of the analysis error of sea surface height anomaly, which corresponds to 50 m of the depth variation of 26.5 Sigma-t, averaged in the upstream region may be enough for the bifurcation of the Kuroshio path forecasts in the ensemble.

[34] The present study suggests the importance of the local eddy dynamics in the Kuroshio recirculation region to the bifurcation of the Kuroshio path. The strong anticyclonic eddy may trigger the intensified eddy-Kuroshio interaction associated with the large-meander formation, whose energy source might be the available potential energy of the Kuroshio and its recirculation system accumulated over the whole Shikoku Basin. However, detailed mechanism is still unclear. Further intensive studies are needed on interactions between the Kuroshio and meso-scale eddies.

[35] The ensemble forecast is a promising way to study predictability of the Kuroshio path. Further development of

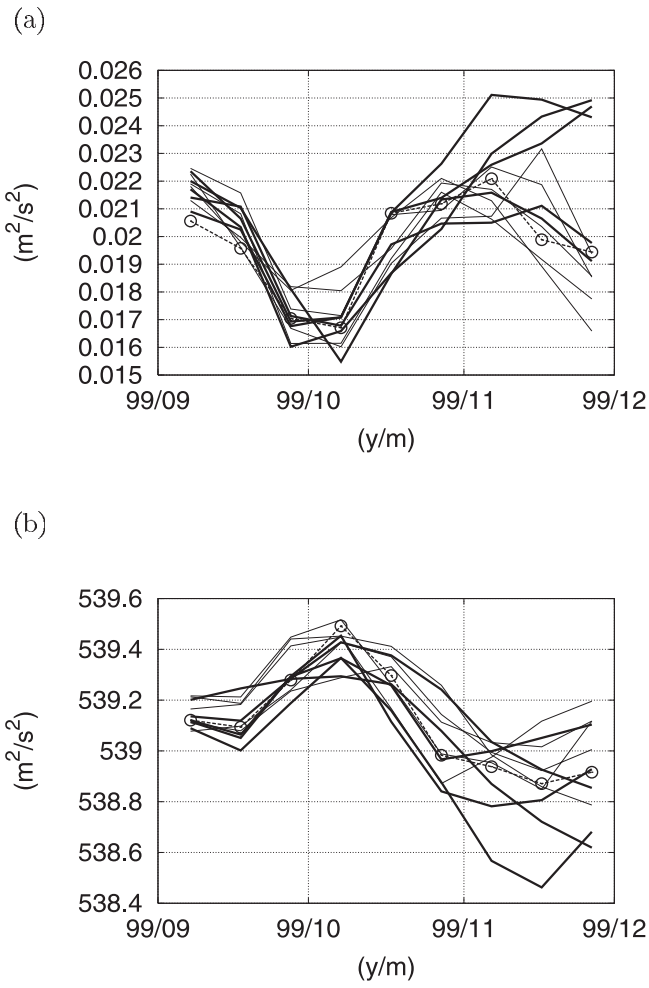

Figure 14. (a) As in Figure 13a except for averaged over the Shikoku Basin, 27°N–35°N, 131°E–141°E. (b) As in Figure 14a except for available potential energy (in m^2 s^{-2}).

the ensemble forecast method [e.g., *Yamane and Yoden*, 2001] would lead us to deeper understanding of the Kuroshio path variation.

Appendix A: Weight of Correction for the Analysis Equation

[36] Following *Mellor and Ezer* [1991], we derive the equation (2). The errors of the observed and forecast sea surface height anomaly (SSHA) are defined according to

$$\Delta\eta^o - \Delta\eta^t = \delta\eta^o, \qquad \Delta\eta^f - \Delta\eta^t = \delta\eta^f. \tag{A1}$$

On the other hand, the errors arising from our assimilation adjustment (analysis) described in equation (1) are defined according to

$$T^a - T^t = \delta T^f + P_{T\eta}\left(F_{T\eta}\left(\Delta\eta^o - \Delta\eta^f\right) + \delta T^C\right), \tag{A2}$$

where δT^C is an error associated with the incomplete correlation between SSH and temperature/salinity, and $\delta T^f = T^f - T^t$. Using equations (A1) and (A2), the assimilation adjustment error variance $\langle (T^a - T^t)^2 \rangle$ is expressed as follows:

$$\left\langle (T^a - T^t)^2 \right\rangle = \left\langle \delta T^{f^2} \right\rangle + P_{T\eta}^2 \left(F_{T\eta}^2 \left(\left\langle \delta\eta^{o^2} \right\rangle + \left\langle \delta\eta^{f^2} \right\rangle \right) + \left\langle \delta T^{c^2} \right\rangle \right) - 2P_{T\eta} F_{T\eta} \left\langle \delta\eta^f \delta T^f \right\rangle. \tag{A3}$$

In the derivation of equation (A3), the forecast, observation and correlation errors are assumed to be uncorrelated.

[37] To determine the weight $P_{T\eta}$, we minimize the adjustment error given in equation (A3) by looking into the condition $\dfrac{\partial \left\langle (T^a - T^t)^2 \right\rangle}{\partial P_{T\eta}} = 0$, which leads to

$$P_{T\eta} = \frac{F_{T\eta} \left\langle \delta\eta^f \delta T^f \right\rangle}{F_{T\eta}^2 \left(\langle \delta\eta^{o^2} \rangle + \langle \delta\eta^{f^2} \rangle \right) + \langle \delta T^{c^2} \rangle}. \tag{A4}$$

Using further assumption of the form

$$\left\langle \delta\eta^f \delta T^f \right\rangle = F_{T\eta} \left\langle \delta\eta^{f^2} \right\rangle \tag{A5}$$

and the derivation of the correlation error [*Mellor and Ezer*, 1991]

$$\left\langle \delta T^{C^2} \right\rangle = F_{T\eta}^2 \left\langle \Delta\eta^{t^2} \right\rangle \left({}^1\!/_{C_{T\eta}^2} - 1 \right), \tag{A6}$$

we can write

$$P_{T\eta} = \frac{\left\langle \delta\eta^{f^2} \right\rangle}{\langle \delta\eta^{o^2} \rangle + \langle \delta\eta^{f^2} \rangle + \langle \Delta\eta^{t^2} \rangle \left({}^1\!/_{C_{T\eta}^2} - 1 \right)}, \tag{A7}$$

where $\langle \Delta\eta^{t^2} \rangle$ is variance of true SSHA. Normalization of the error variances in equation (A7) gives equation (2).

[38] **Acknowledgments.** This work is part of the Japan Coastal Ocean Predictability Experiment (JCOPE) started in October 1997 under the initiative of the Frontier Research System for Global Change (FRSGC), which is supported jointly by Japan Aerospace Exploration Agency (JAXA) and Japan Agency for Marine-Earth Science and Technology (JAMSTEC). We are very thankful to two anonymous reviewers for their constructive comments on the earlier versions of the manuscript. Comments by Hirofumi Sakuma also helped in improving the original manuscript.

References

Boyer, T. P., and S. Levitus (1997), *Objective Analyses of Temperature and Salinity for the World Ocean on a 1/4° Grid*, *NOAA Atlas NESDIS 11*, Natl. Oceanic and Atmos. Admin., Silver Spring, Md.

Cushman-Roisin, B. (1986), Frontal geostrophic dynamics, *J. Phys. Oceanogr.*, *16*, 132–143.

Cushman-Roisin, B., G. G. Sutyrin, and B. Tang (1992), Two-layer geostrophic dynamics: Part I. Governing equations, *J. Phys. Oceanogr.*, *22*, 117–126.

Ebuchi, N., and K. Hanawa (2000), Mesoscale eddies observed by TOLEX-ADCP and TOPEX/Poseidon altimeter in the Kuroshio recirculation region south of Japan, *J. Oceanogr.*, *56*, 43–57.

Ebuchi, N., and K. Hanawa (2003), Influence of mesoscale eddies on variations of the Kuroshio path south of Japan, *J. Oceanogr.*, *59*, 25–36.

Emery, W. J., W. G. Lee, and L. Magaard (1984), Geographical and seasonal distributions of Brunt-Vaisala frequency and Rossby radii in the North Pacific and North Atlantic, *J. Phys. Oceanogr.*, *14*, 294–317.

Endoh, T., and T. Hibiya (2001), Numerical simulation of the transient response of the Kuroshio leading to the large meander formation south of Japan, *J. Geophys. Res.*, *106*, 26,833–26,850.

Evensen, G. (1994), Sequential data assimilation with a nonlinear quasi-geostrophic model using Monte Carlo methods to forecast error statistics, *J. Geophys. Res.*, *99*, 10,143–10,162.

Guo, X., H. Hukuda, Y. Miyazawa, and T. Yamagata (2003), A triply nested ocean model simulating the Kuroshio–Roles of horizontal resolution on JEBAR, *J. Phys. Oceanogr.*, *33*, 146–169.

Hurlburt, H. E., A. J. Wallcraft, W. J. Schmitz Jr., P. J. Hogan, and E. J. Metzger (1996), Dynamics of the Kuroshio/Oyashio current system using eddy-resolving models of the North Pacific Ocean, *J. Geophys. Res.*, *101*, 941–976.

Kalnay, E., et al. (1996), The NCEP/NCAR 40-Year Reanalysis Project, *Bull. Am. Meteorol. Soc.*, *77*, 437–471.

Kamachi, M., T. Kuragano, S. Sugimoto, K. Yoshida, T. Sakurai, T. Nakano, N. Usui, and F. Uboldi (2004), Short-range prediction experiments with operational data assimilation system for the Kuroshio south of Japan, *J. Oceanogr.*, *60*, 269–282.

Kawabe, M. (1995), Variations of current path, velocity, and volume transport of the Kuroshio in relation with the large meander, *J. Phys. Oceanogr.*, *25*, 3103–3117.

Kawai, H. (1969), Statistical estimation of isotherms indicative of the Kuroshio axis, *Deep Sea Res.*, *16*, Suppl., 109–115.

Komori, N., T. Awaji, Y. Ishikawa, and T. Kuragano (2003), Short-range forecast experiments of the Kuroshio path variabilities south of Japan using TOPEX/Poseidon altimetric data, *J. Geophys. Res.*, *108*(C1), 3010, doi:10.1029/2001JC001282.

Kuragano, T., and M. Kamachi (2000), Global statistical space-time scales of oceanic variability estimated from the TOPEX/Poseidon altimetry data, *J. Geophys. Res.*, *105*, 955–974.

Levitus, S., R. Burgett. and,T. P. Boyer (1994), *World Ocean Atlas*, vol. 3, *Salinity*, *NOAA Atlas NESDIS 3*, Natl. Oceanic and Atmos. Admin., Silver Spring, Md.

Lillibridge, J., L. Robert, and F. Vossepoel (1997), Real-time altimetry from ERS-2, paper presented at 3rd ERS Symposium, Eur. Space Agency, Florence, Italy.

Masuda, A. (1982), An interpretation of the bimodal character of the stable Kuroshio path, *Deep Sea Res.*, *29*, 471–484.

Mellor, G. L. (1998), Users guide for a three-dimensional, primitive equation, numerical ocean model, technical report, Princeton Univ., Princeton, N. J.

Mellor, G. L., and T. Ezer (1991), A Gulf Stream model and an altimetry assimilation scheme, *J. Geophys. Res.*, *96*, 8779–8795.

Miller, R. N., and L. L. Ehret (2002), Ensemble generation for models of multimodal systems, *Mon. Weather Rev.*, *30*, 2313–2333.

Mitsudera, H., and R. Grimshaw (1994), Capture and resonant forcing of solitary waves by the interaction of a baroclinic current with topography, *J. Phys. Oceanogr.*, *24*, 2217–2244.

Mitsudera, H., T. Waseda, Y. Yoshikawa, and B. Taguchi (2001), Anticyclonic eddies and Kuroshio meander formation, *Geophys. Res. Let.*, *28*, 2025–2028.

Miyazawa, Y., X. Guo, and T. Yamagata (2004), Roles of meso-scale eddies in the Kuroshio paths, *J. Phys. Oceanogr.*, *34*, 2203–2222.

Murphy, J. M. (1988), The impact of ensemble forecasts on predictability, *Q. J. R. Meteorol. Soc.*, *114*, 463–493.

Pedlosky, J. (1987), *Geophysical Fluid Dynamics*, 2nd ed., 710 pp., Springer, New York.

Qiu, B., and W. Miao (2000), Kuroshio path variations south of Japan: Bimodality as a self-sustained internal oscillation, *J. Phys. Oceanogr.*, *30*, 2124–2137.

Rosati, A., and K. Miyakoda (1988), A general circulation model for upper ocean simulation, *J. Phys. Oceanogr.*, *18*, 1601–1626.

Takano, S. (2002), Application technique of ensemble prediction (in Japanese), *Meteorol. Res. Note*, *201*, 73–103.

Toth, Z., and E. Kalnay (1993), Ensemble forecasting at NMC: The generation of perturbations, *Bull. Am. Meteorol. Soc.*, *74*, 2317–2330.

White, W. B., and J. P. McCreary (1976), On the formation of the Kuroshio meander and its relationship to the large-scale ocean circulation, *Deep Sea Res.*, *23*, 33–47.

Williams, G. P., and T. Yamagata (1984), Geostrophic regimes, intermediate solitary vortices and Jovian eddies, *J. Atmos. Sci.*, *41*, 453–478.

Yamagata, T., and S. Umatani (1987), The capture of current meander by coastal geometry with possible application to the Kuroshio Current, *Tellus, Ser. A*, *39*, 161–169.

Yamagata, T., and S. Umatani (1989), Geometry-forced coherent structures as a model of the Kuroshio large meander, *J. Phys. Oceanogr.*, *19*, 130–138.

Yamane, S., and S. Yoden (2001), Finite-time evolution of small perturbations superposed on a chaotic solution: Experiment with an idealized barotropic model, *J. Atmos. Sci.*, *58*, 1066–1078.

X. Guo, Center for Marine Environmental Studies, Ehime University, 2-5 Bunkyo-cho, Matsuyama, Ehime, 790-8577, Japan.

Y. Miyazawa, Frontier Research Center for Global Change/JAMSTEC, 3173-25 Showamachi, Kanazawa-ku, Yokohama, Kanagawa 236-0001, Japan. (miyazawa@jamstec.go.jp)

T. Yamagata, Department of Earth and Planetary Science, Graduate School of Science, University of Tokyo, 7-3-1 Hongo, Bunkyo-ku, Tokyo, 113-0033, Japan.

S. Yamane, Department of Environmental Security, Faculty of Risk and Crisis Management, Chiba Institute of Science, 3 Shiomi-cho, Choshi, Chiba, 288-0025, Japan.